CHAPTER ONE

Lipid Nanodiscs as a Tool for High-Resolution Structure Determination of Membrane Proteins by Single-Particle Cryo-EM

Rouslan G. Efremov*[,1], Christos Gatsogiannis[†,1], Stefan Raunser[†,1]
*Vrije Universiteit Brussel, Brussels, Belgium
[†]Max Planck Institute of Molecular Physiology, Dortmund, Germany
[1]Corresponding authors: e-mail address: rouslan.efremov@vib-vub.be; christos.gatsogiannis@mpi-dortmund.mpg.de; stefan.raunser@mpi-dortmund.mpg.de

Contents

Abstract

The "resolution revolution" in electron cryomicroscopy (cryo-EM) profoundly changed structural biology of membrane proteins. Near-atomic structures of medium size to large membrane protein complexes can now be determined without crystallization. This significantly accelerates structure determination and also the visualization of small bound ligands. There is an additional advantage: the structure of membrane proteins can now be studied in their native or nearly native lipid bilayer environment. A popular lipid bilayer mimetic are lipid nanodiscs, which have been thoroughly characterized and successfully utilized in multiple applications. Here, we provide a guide for using lipid nanodiscs as a tool for single-particle cryo-EM of membrane proteins. We discuss general methodological aspects and specific challenges of protein reconstitution into lipid nanodiscs and high-resolution structure determination of the nanodisc-embedded complexes. Furthermore, we describe in detail case studies of two successful applications of nanodiscs in cryo-EM, namely, the structure determination of the rabbit

Methods in Enzymology, Volume 594
ISSN 0076-6879
http://dx.doi.org/10.1016/bs.mie.2017.05.007

© 2017 Elsevier Inc.
All rights reserved.

ryanodine receptor, RyR1, and the pore-forming TcdA1 toxin subunit from *Photorhabdus luminescens*. We discuss cryo-EM-specific hurdles concerning sample homogeneity, distribution of reconstituted particles in vitreous ice, and solutions to overcome them.

1. INTRODUCTION

It is predicted that ~23% of human genes code for membrane proteins (Uhlén et al., 2015). Because of their surface accessibility and central importance in many cellular mechanisms, they are attractive drug targets. Thus, in 2006, membrane proteins constituted more than 60% of all known drug targets (Overington, Al-Lazikani, & Hopkins, 2006).

Structural information is key for understanding the interaction between membrane proteins, in particular receptors, and small drug molecules in atomic detail. However, structural investigations on membrane proteins are also important to understand essential cellular mechanisms, including signaling, transport, and energy conversion at the molecular level.

While some structures have been obtained by electron crystallography (Raunser & Walz, 2009) and solution NMR (Hiller & Wagner, 2009), the majority of membrane protein structures has been determined by X-ray crystallography (Vinothkumar & Henderson, 2010). Although the structure of the first membrane protein was solved in 1985 (Deisenhofer, Epp, Miki, Huber, & Michel, 1985), membrane proteins have remained a challenge for structural biology over the past decades. Besides difficulties in obtaining ordered crystals in the case of crystallography, major bottlenecks have been the expression, solubilization, and purification of sufficient amounts of recombinant and biologically active membrane proteins. In recent years, significant progress has been made to overcome these chalenges, and many structures of important membrane proteins have been solved. These include transporters, respiratory complexes, G-protein-coupled receptors (GPCRs), ion channels, and adventitious membrane proteins (Vinothkumar & Henderson, 2010).

However, in many cases, in particular for mammalian membrane proteins, crystals of sufficient quality have not been obtained. Recently, the introduction of a new generation of direct electron detectors (McMullan, Faruqi, Clare, & Henderson, 2014) and the parallel development of image-processing software (Brilot et al., 2012; Li et al., 2013) increased the resolution limit of single-particle electron cryomicroscopy (cryo-EM)

to atomic resolution. Cryo-EM of the post-"resolution revolution" era, as Werner Kühlbrandt coined it (Kühlbrandt, 2014), allows now for the direct structure determination of proteins to near-atomic resolution (between 3 and 4 Å) without crystallization. Consequently, this new development has had a major impact on structural biology, and many structures of mammalian protein complexes that resisted crystallization so far have been determined in the last 3 years. Good examples are γ-secretase (Bai et al., 2015), respiratory complex I (Fiedorczuk et al., 2016; Zhu, Vinothkumar, & Hirst, 2016) and supercomplexes (Letts, Fiedorczuk, & Sazanov, 2016; Wu, Gu, Guo, Huang, & Yang, 2016), ATP synthase (Allegretti et al., 2015), different ions channels (Liao, Cao, Julius, & Cheng, 2013; Wu, Yan, et al., 2016), and transporters (Kim et al., 2015).

As for X-ray crystallography, pure protein samples are needed for single-particle cryo-EM studies. Typically, purification protocols for membrane proteins start with extracting the transmembrane proteins from membranes by solubilizing them in detergents. Protein purification by means of different techniques, mainly affinity and size-exclusion chromatography (SEC), are also performed in the presence of detergent to prevent the precipitation of the protein. Detergent-solubilized membrane proteins can be directly used for single-particle cryo-EM. Since cryo-EM allows observing individual unrestrained protein molecules embedded in a thin layer of amorphous ice, there are no restrictions on choosing a suitable detergent, which is usually not the case in crystallography. For the same reason, detergent-free systems can also be used to study the structures of membrane proteins. Among these systems are polymers such as amphipols (Popot et al., 2011) and styrene–maleic acid (SMA) copolymers (Scheidelaar et al., 2015), which can substitute detergents, or lipid-based systems, such as lipid nanodiscs (Schuler, Denisov, & Sligar, 2013), a saposin-lipoprotein nanoparticle system (e.g., Salipro®, EP 2745834 B1) (Frauenfeld et al., 2016), and even liposomes (Wang & Sigworth, 2010).

Since detergents must be used at concentration levels above the critical micelle concentration (CMC) to prevent precipitation of the protein, their concentration in the solution is high enough to decrease the contrast of cryo-EM images (Schmidt-Krey & Rubinstein, 2011). This is not the case when reconstituting membrane proteins in amphipols. Therefore, amphipols have been successfully used for the determination of the first high-resolution structures of the TRPV1 channel (Liao et al., 2013) and γ-secretase (Bai et al., 2015). In general, amphipols are popular polymers for reconstituting membrane proteins in single-particle cryo-EM (Popot

et al., 2011). Although this process is more straightforward than reconstituting proteins into lipid environments, amphipols as well as detergents have the disadvantage that the system does not contain lipids. There are a number of reasons why studying the structure of membrane proteins in a lipid environment has advantages over examining them in detergent.

First of all, the lipid bilayer is the native environment for membrane proteins, and it has significantly different physical properties than its mimetic detergent micelle (Zhou & Cross, 2013). In contrast to planar lipid bilayers, detergent micelles typically have a spherical shape and differ considerably in their dielectric constant and electrostatic potential. In some cases these differences can have severe consequences, resulting in structures of nonnatively folded membrane proteins when crystallized from detergent solution (Cross, Murray, & Watts, 2013; Zhou & Cross, 2013). However, the effects are normally milder and while the proper fold is preserved when the membrane protein is solubilized in detergent or reconstituted in polymers, the protein dynamics, which are more sensitive to the environment than the structure, are very often influenced or altered. For example, the absorption spectrum of bacteriorhodopsin shifts upon solubilization in detergent and its photocycle kinetics are changed (Lam & Packer, 1983), even if its structure remains virtually unaltered. A more recent vivid example is related to the functional dynamics of the rabbit ryanodine receptor 1 (RyR1). Solubilized in Tween-20 (Yan et al., 2015) or CHAPS (Zalk et al., 2015), the structure of the channel is similar to the one determined in a lipid environment (Efremov, Leitner, Aebersold, & Raunser, 2015). However, in Tween-20 it is locked in a closed state and does not open under conditions that induce the full opening of the channel in lipid membranes (Bai, Yan, Wu, Li, & Yan, 2016).

The function of membrane proteins often depends on the direct interaction with lipids (Phillips, Ursell, Wiggins, & Sens, 2009). A layer of annular lipids surrounds the proteins. These lipids are in direct contact with the hydrophobic surface of the protein and tightly seal the membrane at the protein–membrane interface. Often they take distorted arrangements to adapt to the rough surface of the protein (Lee, 2004) and play an important role in stabilizing membrane protein oligomers (Gupta et al., 2017). However, most of the annular lipids are removed during the purification process, and in most cases they are not reintroduced afterward for crystallography or single-particle cryo-EM with detergents or polymers. In many crystal structures (Yeagle, 2014) and also recent cryo-EM structures (Liao et al., 2013) though, some very tightly bound lipid molecules remain bound during purification and can be resolved in the structures.

The optimal way to purify a membrane protein together with its natural annular lipids is to use detergent-free purification procedures that make use of SMA copolymers (Dörr et al., 2014, 2016) or nanodiscs (Civjan, Bayburt, Schuler, & Sligar, 2003). The development of these techniques is still in its infancy, and it has not yet been broadly applied. The most common approach is thus to purify the protein using detergents and reintroduce lipids afterward. In most cases, lipid composition can be varied and adjusted to mimic the natural membrane environment or to identify key lipids and lipid compositions. This has been done, for instance, for bacteriorhodopsin (Lee et al., 2015), the ABC transporter MbsA (Kawai, Caaveiro, Abe, Katagiri, & Tsumoto, 2011), or cytochrome P450 reductase (Das & Sligar, 2009).

Among the different available options for reconstituting membrane proteins in a lipid bilayer, the lipid nanodisc system currently presents the best-understood and -characterized method. Lipid nanodiscs were developed in the laboratory of Stephen Sligar (Bayburt & Sligar, 2003). They are composed of a patch of lipid bilayer, which is surrounded by membrane scaffold protein (MSP). MSP is a derivative form of apolipoprotein A-1 (Apo-A1) (Ritchie et al., 2009) and composed of short amphipathic helices. In an assembled nanodisc, two MSPs arrange in a parallel or antiparallel manner, forming a belt around the hydrophobic region of the lipid bilayer that includes a few hundred lipid molecules (Fig. 1). Constructs of MSP with

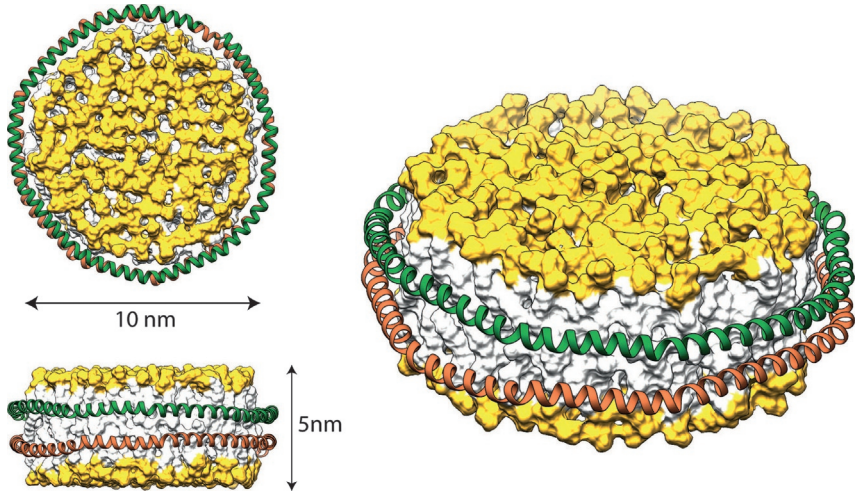

Fig. 1 Model of MSP1–POPC nanodisc structure. The two copies of MSP, surrounding the phospholipid bilayer, are shown in *green* and *brown*. Lipid headgroups are colored in *yellow*. The model was produced using the CHARMM-GUI server.

various numbers of amphipathic helices have been designed so that different sizes of nanodiscs can be obtained reaching diameters between ~10 and ~17 nm. This corresponds to ~100–600 lipids per nanodisc (Ritchie et al., 2009; Schuler et al., 2013). While MSP defines the size limits of the nanodiscs, as can be observed by negative stain electron microscopy (EM), the actual dimensions of the reconstituted discs vary significantly (Nasr et al., 2017). A recently reported method to generate covalently circularized nanodiscs using sortase produced significantly more homogeneous nanodiscs with diameters of up to 80 nm (Nasr et al., 2017).

Nanodiscs have shown to be potentially useful in studying membrane protein complexes, in particular fragile temporary signaling complexes, like those formed by GPCRs (Leitz, Bayburt, Barnakov, Springer, & Sligar, 2006). Detergents can disrupt the hydrophobic interactions involved in protein–protein and protein–lipid–protein interactions. For example, the β_2-adrenergic receptor, where mainly two palmitic acid and two cholesterol molecules mediate the interactions between two protomers of the natural dimer, binds only to G-proteins when reconstituted in nanodiscs but not when solubilized in detergents (Leitz et al., 2006). Other examples are the proton pump bacteriorhodopsin (Johnson et al., 2014) the ABC transporters MsbA (Kawai et al., 2011) and MalK (Bao & Duong, 2014). It has been shown that the functional properties of these proteins reconstituted in nanodiscs are similar to those in native membranes (Bao & Duong, 2014; Johnson et al., 2014; Kawai et al., 2011). Nanodiscs have been successfully used to determine high-resolution structures of membrane proteins using solution NMR (Hagn & Wagner, 2015) and single-particle cryo-EM (Efremov et al., 2015; Frauenfeld et al., 2011; Gao, Cao, Julius, & Cheng, 2016; Gatsogiannis et al., 2016; Shen et al., 2016).

Although nanodiscs are capable of mimicking the situation in a native lipid membrane, some biophysical properties of the lipids are slightly different and have to be taken into account when working with nanodiscs. For instance, the phase transition temperatures of lipids are higher and the thermal expansion coefficients of lipids are lower than in liposomes (Denisov, McLean, Shaw, Grinkova, & Sligar, 2005). Molecular dynamics simulations showed that the lipid layer that is in direct contact with MSP is perturbed due to the hydrophobic mismatch between MSP and lipids. However, 15–20 Å away from MSP, corresponding to two layers of lipid molecules, the properties of the lipids were similar to those in a planar bilayer (Schuler et al., 2013; Shih, Denisov, Phillips, Sligar, & Schulten, 2005).

Indeed, it has been shown for the ABC transporter MsbA that its activity is higher in larger nanodiscs containing more lipids (Kawai et al., 2011). EPR experiments with labeled lipids indicated that lipids within nanodiscs are generally more ordered than in liposomes and to some extent resemble a lipid bilayer in the presence of cholesterol (Stepien, Polit, & Wisniewska-Becker, 2015).

Examples of single-particle cryo-EM structures solved of membrane proteins reconstituted into lipid nanodiscs include the early work on the complex between the bacterial ribosome and the SecYE translocon (Frauenfeld et al., 2011), the muscular isoform of the rabbit ryanodine receptor (RyR1) (Efremov et al., 2015), more recent high-resolution studies of the Tc toxin from *Photorhabdus luminescens* (Gatsogiannis et al., 2016), the transient receptor potential channels TRPV1 (Gao et al., 2016) and PKD2 (Shen et al., 2016) (Fig. 2; Table 1). These examples demonstrate the feasibility of high-resolution 3-D structural analysis of membrane proteins embedded in nanodiscs, even with relatively small extracellular domains, as in the case of the transient receptor potential channels. In spite of the heterogeneous shape of the nanodisc, the transmembrane region of the proteins is one of the best-resolved parts of the structures.

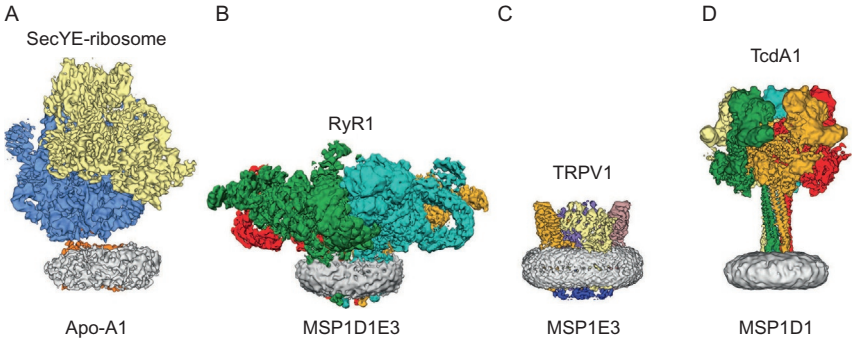

Fig. 2 Cryo-EM structures of proteins reconstituted in nanodiscs. (A–D) Examples of membrane proteins that have been incorporated in nanodiscs and successfully analyzed by cryo-EM include the bacterial ribosome-SecYE complex (7.1 Å, EMD-1858; Frauenfeld et al., 2011) (A), the rabbit ion channel RyR1 in the closed state (6.1 Å, EMD-2751; Efremov et al., 2015) (B), the human ion channel TRPV1 (3.0 Å, EMD-8117; Gao et al., 2016) (C), and the TcdA1 toxin subunit from *P. luminescens* in the pore state (3.5 Å, EMD-4068; Gatsogiannis et al., 2016) (D). The nanodisc density is shown in *gray*. The type of MSP protein used for reconstitution is indicated.

Table 1 Reconstitution conditions for membrane proteins in which medium- to high-resolution single-particle cryo-EM structures were obtained

Protein	Protein solubilizing detergent	MSP construct	Size of protein (total)	Lipids	Lipid/ MSP/ protein molar ratio	Lipid solubilizing detergent	Detergent removal	Reconstitution temperature (°C)	Resolution (Å)	References
SecYE-ribosome	DDM	Apo-A1	SecYEG 74 kDa bound to *E. coli* 70S ribosome (2.4 MDa)	*E. coli* phospholipids	185:11:1	Cholate	Bio-Beads	37	7.1	Frauenfeld et al. (2011)
RyR1	CHAPS	MSP1D1E3	2.3 MDa	POPC	140:2:1	CHAPS	Bio-Beads	4	6.1	Efremov et al. (2015)
TRPV1	DDM	MSP1E3, MSP2N2	330 kDa	Soybean polar lipids extract	600:4:1, 900:6:1, 400:4:1	DDM	Bio-Beads	4	3.2	Gao et al. (2016)
Tc toxin TcdA1	Tween-20	MSP1D1	1.4 MDa	POPC	440:8:1	CHAPS	Dialysis	4	3.5	Gatsogiannis et al. (2016)
PKD2 channel	DDM	MSP2N2	340 kDa	Soybean polar lipids	200:1:1 (or 0.25)	None	Bio-Beads	4	3.0	Shen et al. (2016)

Below, we first describe general considerations and approaches that need to be taken into account when reconstituting membrane proteins into lipid nanodiscs for single-particle cryo-EM. Next, we provide detailed protocols of reconstitution and cryo-EM sample preparation for two proteins, the rabbit ryanodine receptor RyR1 and the TcdA1 subunit of the Tc toxin complex from *P. luminescens*.

2. GENERAL CONSIDERATIONS

Reconstitution of membrane proteins into lipid nanodiscs is a self-assembling process. The most frequently applied method is to mix the purified membrane protein, lipids, and MSP in detergent solution and remove the detergent by dialysis or Bio-Beads (Fig. 3). This approach provides the best control over the reconstitution process and is the most reproducible. Each of the components, as well as the method for depleting the detergent from the solution, influences the assembly process (Ritchie et al., 2009). Therefore, the MSP construct, lipids, and detergents need to be chosen carefully. Single-particle EM studies require structurally homogeneous samples. Hence, the aim is to produce homogeneous nanodiscs with a single reconstituted protein, almost no empty nanodiscs, and no excess of proteins or lipids. To achieve this, the molar ratios between the membrane protein, MSP, and lipids during reconstitution should reflect their composition in the assembled discs.

Another way to reconstitute membrane proteins is to incorporate them into preformed empty nanodiscs. This method is especially suited for

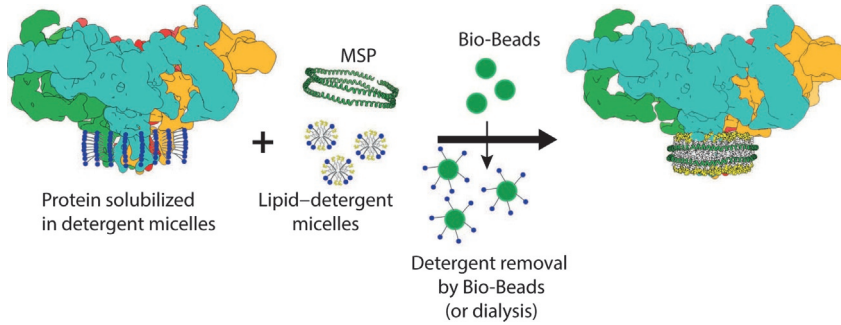

Fig. 3 Schematic of membrane protein reconstitution in nanodiscs. The detergent-solubilized membrane protein, lipids, and MSP are mixed and the detergent is removed by dialysis or adsorption to Bio-Beads. This results in the reconstitution of the membrane protein in nanodiscs.

adventitious membrane proteins, such as pore-forming toxins, that can directly penetrate membranes (Gatsogiannis et al., 2016).

Membrane proteins can also be reconstituted into nanodiscs directly from a detergent-solubilized membrane fraction before protein purification. This direct reconstitution approach has been used on bacterial (Civjan et al., 2003; Duan, Civjan, Sligar, & Schuler, 2004; Marty, Wilcox, Klein, & Sligar, 2013) and eukaryotic (Roy, Pondenis, Fan, & Das, 2015; Shirzad-Wasei et al., 2015) proteins. It can be of advantage for membrane proteins that are unstable in detergent or require weakly bound native lipids for protein function. When using the direct reconstitution approach, the lipid composition and concentration cannot be controlled. This may result in less homogeneous nanodiscs. Furthermore, the additional reconstitution of smaller membrane proteins together with the protein of interest in the same nanodisc cannot be prevented. Since many MSPs not only surround the protein of interest but also other membrane proteins, different concentrations and ratios are needed. In general, the requirements for this method differ from those of the standard approach.

When preparing nanodiscs, an optimal MSP construct that determines the size of the nanodisc should be first selected (see above). Optimally, the nanodisc should be just large enough to accommodate the protein, but keep at least two layers of lipids between protein and MSP to avoid unwanted interactions with the MSP and ensure a proper mimic of the lipid bilayer environment. Too large nanodiscs may result in less homogeneous dimensions of the discs and the "floating" of the protein within the disc (Fig. 5H and section describing TcA reconstitution). This can in turn interfere with particle alignment during image processing. In addition, the larger the nanodiscs, the higher the probability is to reconstitute more than one protein in a disc (Fig. 5F). A range of MSP constructs generated by the Sligar lab (Grinkova, Denisov, & Sligar, 2010) are available from Addgene (www.addgene.org). They allow assembling nanodiscs with diameters ranging from ~10 nm (MSP1D1 construct holding ~100 lipids) up to ~17 nm (MSP2N3 construct surrounding ~600 lipid molecules) (Ritchie et al., 2009; Schuler et al., 2013). The MSPs can be expressed in *Escherichia coli* and purified by affinity chromatography (see Ritchie et al., 2009 for a detailed protocol). MSPs as well as preformed nanodiscs are also commercially available.

The lipids should be chosen based on prior knowledge of the protein's native environment or on previous successful reconstitutions in liposomes or other bilayer systems. Besides total lipid extracts, for example, total *E. coli* or

soybean lipid extracts (Gao et al., 2016; Hernández-Rocamora, García-Montañés, Rivas, & Llorca, 2012; Ritchie et al., 2009), mostly synthetic lipids have been successfully used. In particular, zwitterionic and charged phospholipids like 1,2-dimyristoyl-*sn*-glycero-3-phosphocholine (DMPC), 1-palmitoyl-2-oleoyl-*sn*-glycero-3-phosphocholine (POPC), 1,2-dipalmitoyl-*sn*-glycero-3-phosphocholine (DPPC), 1-palmitoyl-2-oleoyl-*sn*-glycero-3-phosphoserine (POPS), 1,2-dioleoyl-*sn*-glycero-3-phosphoserine (DOPS), 1,2-dimyristoyl-*sn*-glycero-3-phosphoglycerol (DMPG), and 1-palmitoyl-2-oleoyl-*sn*-glycero-3-phosphoglycerol (POPG) alone or in mixture have achieved good results (Bao, Dalal, Wang, Rouiller, & Duong, 2013; Nasr & Singh, 2014; Orlando et al., 2014; Ritchie et al., 2009; Wadsäter et al., 2013). The gel-to-liquid phase transition temperature of the lipid bilayer is an important parameter to consider when preparing nanodiscs. The lipid bilayer should be in the liquid phase under experimental conditions, while optimal reconstitution occurs at temperatures around the phase transition temperature.

Sodium cholate is the most commonly used detergent for producing nanodiscs (Ritchie et al., 2009). Even though the protein is solubilized in another detergent, it is normally used for solubilizing the lipids (Bayburt, Grinkova, & Sligar, 2006) and for reconstituting proteins in preformed nanodiscs (Gatsogiannis et al., 2016). The presence of sodium cholate, however, should not interfere with protein stability. Alternatively other detergents have been used to solubilize lipids, namely, *n*-dodecyl-β-D-maltoside (DDM) (Boldog et al., 2006), CHAPS (Efremov et al., 2015), *n*-octyl-β-D-glucopyranoside (OG) (Justesen et al., 2013), Triton X-100 (Mi et al., 2008), and digitonin (Eggensperger, Fisette, Parcej, et al., 2014).

For an optimal reconstitution, the protein:MSP:lipid ratio should exactly match the composition of the nanodiscs and the protein:MSP molar ratio should be kept at 1:2 unless an excess of empty nanodiscs is desired.

The optimal amount of lipids to reach a certain diameter of empty nanodiscs has been experimentally determined for some MSP constructs and common synthetic lipids (see table 11.2 in Ritchie et al., 2009). When a membrane protein is reconstituted, the number of lipids should be adjusted to account for the lipids displaced by the protein. To estimate the membrane cross-section of an α-helical membrane protein, one can assume an area of $\sim 140\,\text{Å}^2$ per transmembrane helix (Ritchie et al., 2009). Phospholipids occupy, respectively, an area of 52, 57, and $69\,\text{Å}^2$ per molecule for DPPC, DMPC, and POPC (Nagle & Tristram-Nagle, 2000).

Thus the number of lipid molecules per nanodisc can be estimated as such:

$$N_{\mathrm{lip}} = 2^{*}\left(S_{\mathrm{ND}} - S_{\mathrm{prot}}\right)/S_{\mathrm{lip}}$$

N_{lip} is the number of lipids per nanodisc, S_{ND} is the surface area of the lipid nanodisc, S_{prot} is the area of the protein's transmembrane section, and S_{lip} is the area occupied by one phospholipid molecule. Since membranes are lipid bilayers, a factor of two has to be introduced.

The surface area of the lipid nanodisc can be estimated from the number of amino acids, M, in MSP using the empirical formula (Denisov, Grinkova, Lazarides, & Sligar, 2004):

$$S_{\mathrm{ND}} = (0.423^{*}M - 9.75)^{2}\left(\mathrm{\AA}^{2}\right)$$

The approximate membrane cross-section of a protein with N_{TM} transmembrane helices is

$$S_{\mathrm{prot}} = 140^{*}N_{\mathrm{TM}}\left(\mathrm{\AA}^{2}\right)$$

The reconstitution process is initiated by removing the detergent using Bio-Beads or dialysis lasting from few hours up to several days at temperatures between 4°C and 37°C. Reconstitution is optimally performed close to the phase transition temperature of lipids (Ritchie et al., 2009). High glycerol concentrations in the buffer should be avoided since glycerol interferes with the reconstitution process at concentrations above 4% (Ritchie et al., 2009). It is often useful to analyze the reconstituted nanodisc by SEC. A clear peak corresponding to the reconstituted protein should be observed and if both protein and lipid concentrations are measured in the peak, they should closely correspond to the calculated protein:lipid ratio. If the reconstituted protein is to be further used for structural studies, the homogeneity of the nanodisc dimensions should be determined using, for example, negative stain EM and/or cryo-EM. The absence of aggregates, liposomes, and homogeneous dimensions of the protein particles indicates a successful reconstitution (Figs. 4A and 5D–F). In practice, however, it is difficult to obtain completely homogenous nanodiscs (Nasr et al., 2017) and a certain degree of inhomogeneity has to be taken into account during cryo-EM image processing. In the case of the magnesium channel CorA, for example, inhomogeneity of nanodiscs interfered with particle alignment and precluded a high-resolution 3-D reconstruction (Matthies et al., 2016).

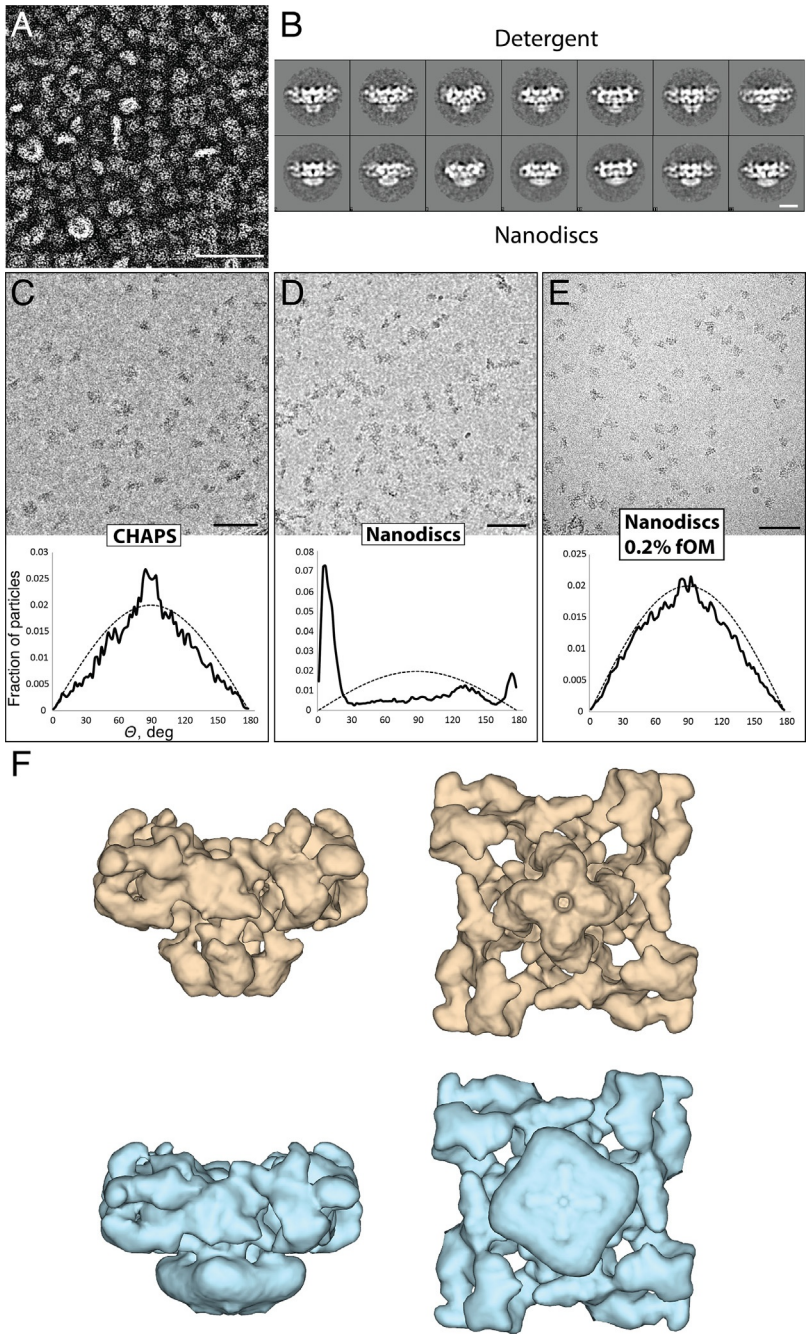

Fig. 4 Single-particle EM of RyR1 reconstituted into lipid nanodiscs. (A) An image of negatively stained RyR1 reconstituted into lipid nanodiscs. It shows an example of sub-optimal reconstitution resulting in small liposome-like structures and large elongated

(Continued)

If the reconstitution is not optimal, the following parameters can be varied: the amount and type of the lipids, the MSP construct, and the detergent. In addition, the temperature and rate at which the detergent is removed can be modified. The optimal protein:MSP:lipid ratio needs to be fine-tuned by scanning various ratios around the calculated one. An alternative approach is to perform the reconstitution under conditions that result in an excess of empty nanodiscs (Table 1) followed by affinity and/or SEC to remove empty nanodiscs (Fig. 5F).

3. SINGLE-PARTICLE CRYO-EM OF THE RYANODINE RECEPTOR RyR1 RECONSTITUTED INTO LIPID NANODISCS

In the following paragraph, we describe how we reconstituted the rabbit ryanodine receptor RyR1 into lipid nanodiscs and determined its structure using single-particle cryo-EM. Ryanodine receptors (RyRs) are tetrameric cation channels with high conductance (Yuchi & Van Petegem, 2016) that reside in the sarcoplasmic or endoplasmic reticulum (SR, ER). RyRs play a central role in muscular contraction, where the channels control calcium release from the SR, initiating muscle contraction. RyRs are gated by Ca^{2+} and through direct interaction with the voltage-gated calcium channel, $Ca_v1.1$ (Wu, Yan, et al., 2016), which resides in the cytoplasmic membrane. The gating of RyRs is tuned by interaction with multiple small molecules and proteins (Van Petegem, 2014). RyRs are the largest known ion channels with a molecular weight of 2.3 MDa for the

Fig 4—cont'd or discoid lipidic structures along with densely packed particles of RyR1. (B) 2-D class averages of vitrified RyR1 displaying side views of the channel solubilized in CHAPS or reconstituted into lipid nanodiscs. Additional density surrounding the transmembrane domain corresponds to nanodiscs. Scale bar, 10 nm. (C–E) Cryo-EM images and angular distribution of RyR1 solubilized in CHAPS (C), or reconstituted in nanodiscs (D), or reconstituted in nanodiscs and vitrified in the presence of 0.2% fluorinated octyl maltoside (E). Distribution of the angle between the fourfold symmetry axis of RyR1 and the normal of the sample plane is shown as a plot for each condition. The Θ distribution for particles with random orientations is described by $\sin\Theta$ shown in the plots using a *dashed line*. Scale bars, 100 nm. (F) 3-D reconstructions of RyR1 solubilized in CHAPS (*brown*) and reconstituted in nanodiscs (*cyan*) show that the density corresponding to the nanodisc is *square with rounded corners*. The cryo-EM images were acquired on a JEOL JEM 3200 TEM, operated at 200 kV on a CMOS TVIPS F816 camera and processed in SPARX (Hohn et al., 2007).

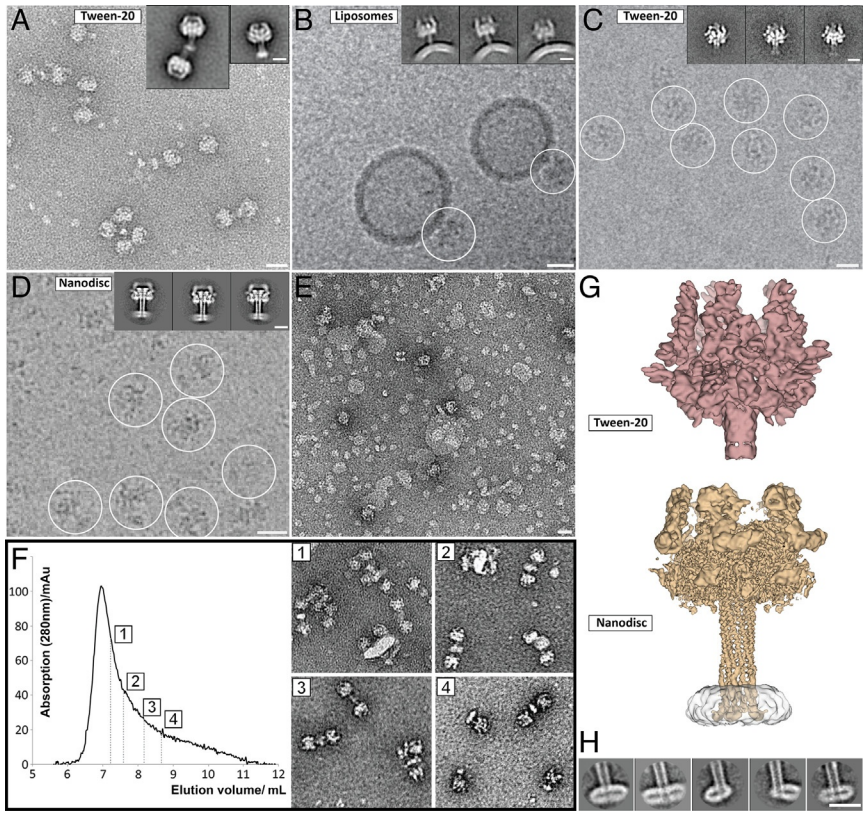

Fig. 5 Single-particle EM of the TcdA1 pore complex embedded in lipid nanodiscs. (A) Typical micrograph area of the negatively stained TcdA1 pore, induced at pH 11 in the presence 0.05% Tween-20. Note that complexes aggregate at the tip of the channel, which is the hydrophobic transmembrane region. The *insets* show representative class averages of one or two tip-to-tip-oriented TcdA1 complexes. (B–D) Typical subareas of cryo-EM images of TcdA1 pores embedded in liposomes (B), in the presence of Tween-20 (C), and reconstituted in lipid nanodiscs (D). Some particles are highlighted with *white circles*. *Insets* show representative class averages. (E) Typical micrograph area of negatively stained TcdA1 embedded into lipid nanodiscs, as an example of a suboptimal protein:MSP ratio. Note the excess of empty nanodiscs and small liposome-like structures. (F) Gel filtration chromatogram of TcdA1 reconstituted in lipid nanodiscs. Fractions used for EM are marked by *dashed lines*, and typical micrograph areas are shown. (G) 3-D volumes of TcdA1 in Tween-20 (*pink*) and TcdA1 reconstituted in nanodiscs (*brown*). Note the absence of the transmembrane domain in the Tween-20 reconstruction of the pore state. Cryo-EM images of TcdA1 in Tween-20 and nanodiscs were taken on a JEOL JEM 3200 EM operated at 200 kV on a CMOS TVPIS F816 camera and a FEI Titan Krios operated at 300 kV on a Falcon II direct detector, respectively. (H) 2-D classification of TcdA1 reconstituted into lipid nanodiscs focused on the transmembrane domain. Note the variability in the diameter of the nanodisc and position of the transmembrane domain relative to the nanodisc. Scale bars for micrographs and class averages are, respectively, 20 and 10 nm.

tetramer. The square-shaped cytoplasmic domain of the channel constitutes 80% of the protein and has an edge length of ~270 Å (Van Petegem, 2014).

For many years, the skeletal muscle isoform RyR1 from rabbit has been a model specimen for single-particle cryo-EM. The most common purification protocol of RyR1 uses a mixture of CHAPS with phospholipids to keep the protein in a stable and active form (Hawkes, Díaz-Muñoz, & Hamilton, 1989). For single-particle cryo-EM, the lipids were removed shortly before plunge-freezing to improve the image contrast (Samsó, Feng, Pessah, & Allen, 2009; Samsó, Wagenknecht, & Allen, 2005). Our primary motivation for reconstituting RyR1 into lipid nanodiscs for single-particle cryo-EM was to leave it in a lipid environment in order to ensure the active conformation of the protein. At the time, only low- to medium-resolution structures of RyR1 were available (Samsó et al., 2005). The number of transmembrane helices was not known and we could only estimate the diameter of the transmembrane region. Since its largest dimensions are between ~100 and ~110 Å, we chose the MSP1D1E3 construct, which forms nanodiscs with a diameter of ~12 nm (Denisov et al., 2004), for the reconstitution.

We decided to use the synthetic phospholipid POPC for the nanodiscs because it is a common lipid for reconstituting membrane proteins and its phase transition temperature of −2°C (https://avantilipids.com/tech-support/physical-properties/phase-transition-temps/) is close to the temperature at which we typically work with the protein.

We calculated the number of lipids per nanodisc as follows:

$$N_{\mathrm{lip}} = \pi/4\left(D_{\mathrm{ND}}{}^2 - D_{\mathrm{RyR1}}{}^2\right)$$

Here, D_{ND} is the diameter of the nanodisc (120 Å), and D_{RyR1} is the average diameter of the membrane-embedded part of RyR1 (90 Å). This results in a membrane area of ~5000 Å^2 corresponding to ~145 POPC lipids per nanodisc. We have provided a detailed description of the reconstitution protocol:

- RyR1 was purified by solubilizing SR membranes in CHAPS in the presence of soy lecithin following SEC and sucrose gradient centrifugation. The excess of lipids was removed by an additional SEC in 0.8% CHAPS without lipids (see Efremov et al., 2015 for details).
- POPC, solubilized in chloroform, was purchased from Avanti Polar Lipids (USA). After evaporating the solvent under a stream of nitrogen, the phospholipid was rehydrated in 10 m*M* MOPS, pH 7.4 at a

concentration of 10 mg/mL. The lipid stock solution was frozen and stored in aliquots at −80°C.

- Prior to the reconstitution process, POPC was solubilized at a concentration of 3.8% (42 m*M*) in 10 m*M* MOPS, pH 7.4, 150 m*M* NaCl, and 8.5% CHAPS.
- MSP1E3D1 was expressed in *E. coli* using the pET expression system and purified using Ni-NTA affinity chromatography. A detailed protocol can be found elsewhere (Ritchie et al., 2009). Afterward, MSP was dialyzed overnight against 20 m*M* MOPS, pH 7.4, 100 m*M* NaCl at 4°C. The purified protein was then incubated overnight with TEV proteases at a ratio of 1:200 (w/w) MSP:TEV in the presence of 1 m*M* DTT in order to cleave the His-tag. Subsequently, the TEV proteases and cleaved peptide were removed by passage through a Ni-NTA column. Concentrated to ∼10 mg/mL, MSP was aliquoted and stored at −80°C until used.
- Reconstitution was accomplished by mixing 400 n*M* (0.9 mg/mL) solubilized RyR1, 800 n*M* MSP (0.026 mg/mL) and 56 μ*M* (0.043 mg/mL) POPC in 20 m*M* MOPS, pH 7.4, 700 m*M* NaCl, 2 m*M* DTT, 1 m*M* EGTA, 10% sucrose, and 0.5% CHAPS. The mixture was incubated for 2 h at 4°C.

Next, the detergent was removed by adsorption to Bio-Beads (Bio-Rad) overnight at 4°C. The capacity of Bio-Beads to absorb different detergents has been tabulated by Rigaud et al. (Lévy et al., 1999). To ensure complete detergent absorption, we added two to three times more Bio-Beads than the theoretical calculated amount.

To ensure that all the detergent is removed by Bio-Beads, the concentration of the detergent in the protein solution needs to be measured beforehand by, for example, a colorimetric assay (Urbani & Warne, 2005) and the amount of Bio-Beads adjusted accordingly. This is particularly important for detergents with a low CMC. In this case, the protein-bound detergent constitutes the major part of the total amount of detergent (Crichton et al., 2013; Ilgü et al., 2014). Care should be taken that not too excessive amounts of Bio-Beads are used because they can absorb lipids along with the detergent (Lévy et al., 1999).

We first visualized reconstituted RyR1 by negative stain EM, which showed that the protein had the expected tetrameric shape, and aggregates or liposomes were absent (Fig. 4A). RyR1 in nanodiscs was then plunge-frozen using a cryoplunge CP3 (Gatan) following a standard protocol: 2 μL of RyR1 in nanodiscs at a concentration of 1–2 mg/mL were applied

onto glow-discharged C-flat CF-1.2/1.3-4C carbon grids (Protochips), automatically blotted from both sides for 1 s and then plunge-frozen.

Cryo-EM images of RyR1 nanodiscs revealed a notable difference in particle distribution compared to the CHAPS-solubilized protein (Fig. 4C and D). In nanodiscs, RyR1 had the tendency to cluster nonspecifically. The most pronounced effect, however, was on the orientation of the particles. Upon reconstitution into nanodiscs, RyR1 was oriented with its symmetry axis perpendicular to the plane of the grid (Fig. 4D). This is detrimental for calculating a 3-D single-particle reconstruction. Surprisingly, the analysis of the particle distribution showed a single strong peak near zero degrees Θ angle (Fig. 4D), indicating that the particles stuck to only one air–water interface instead of being equally distributed in the vitreous ice. We assumed that in the absence of detergent hydrophobic interactions between the soluble regions of the RyR1 molecules were enhanced, resulting in the observed aggregation and strong interaction with the air–water interface. To solve this problem, we screened a number of small molecules that modulate hydrophobic interactions but, unlike detergents, preserve the lipid bilayer. We found that fluorinated octyl maltoside (fOM, Anatrace) resolved the problem when added at a concentration of 0.2%. The particles were then randomly oriented and did not aggregate (Fig. 4E). Due to the lipophobic property of their perfluorinated tails, fluorinated detergents do not solubilize lipid bilayers (Breyton, Chabaud, Chaudier, Pucci, & Popot, 2004). Using negative stain EM, we showed that even at a concentration of 1%, fOM does not solubilize nanodiscs.

During image processing, the nanodiscs became clearly visible in 2-D class averages as an additional density around the membrane region of RyR1 (Fig. 4B). In the case of CHAPS-solubilized RyR1, this density is absent, indicating that the size and therefore the electron scattering density of nanodiscs are significantly larger than that of a detergent micelle. Accordingly, in the 3-D reconstruction the density corresponding to nanodiscs was considerably larger than the one of CHAPS micelles. Unexpectedly, the nanodiscs had a square shape with rounded corners (Fig. 4F). This was also the case for tetrameric TRP ion channels in nanodiscs (Gao et al., 2016). We do not know whether the square shape of the nanodiscs is an artifact of image processing or whether the shape of the nanodiscs adapts to the shape of the reconstituted protein. It has been shown that larger empty nanodiscs can take a noncircular shape at certain lipid:MSP ratios (Nasr et al., 2017). The structures of more membrane proteins with different shapes and

symmetries reconstituted into nanodiscs with different diameters will be needed to answer these open questions.

The horizontal density profile of the nanodisc also corresponds well with the expected density profile of a lipid bilayer. Two high density regions separated by a distance of ~30–35 Å at both surfaces of the bilayer corresponding to phospholipid headgroups and a lower density at the center of the bilayer corresponding to the hydrophobic tails (Fig. 4B).

Finally, in case of RyR1 its structure was determined under three conditions: solubilized in CHAPS (Zalk et al., 2015), solubilized in Tween-20 (Yan et al., 2015), and in nanodiscs (Efremov et al., 2015). The structure of the transmembrane domains under all three conditions is virtually identical when the structures of the closed state determined at resolutions between 3.8 and 6 Å are compared. The data set of RyR1 reconstituted into nanodiscs contained significantly less particles than those of detergent-solubilized proteins, which resulted in a lower resolution of the reconstruction and did not allow resolving protein side chains. The structure of TRPV1 reconstituted into nanodiscs and determined by single-particle cryo-EM (Gao et al., 2016) demonstrated that the high-resolution reconstruction of a transmembrane region embedded into nanodiscs is possible, even for proteins of relatively small dimensions in comparison to the nanodiscs (Fig. 2C). In this study not only protein side chains were well resolved inside the nanodiscs, but also specifically bound lipids and ligands were clearly visualized (Fig. 6), demonstrating the power of nanodiscs for studies of lipid protein interactions in a near-native lipid bilayer environment.

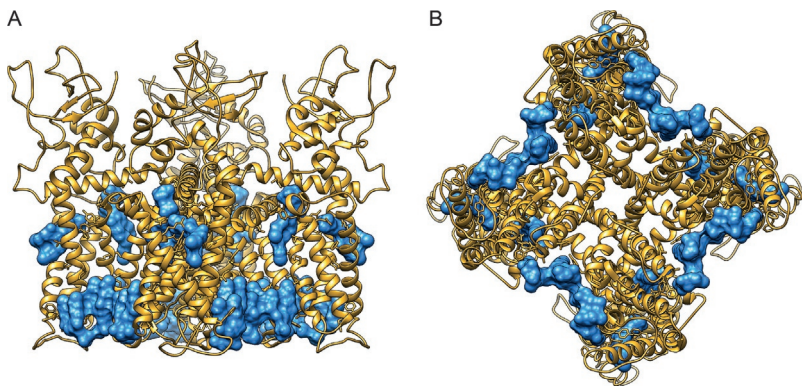

Fig. 6 Annular lipids bound to TrpV1. (A and B) Side (A) and top view (B) of the molecular model of apo TrpV1 depicted as ribbon diagram (*gold*) (PDB-ID: 5IRZ). Annular lipids specifically bound to the protein are shown in surface representation (*blue*).

4. EM ANALYSIS OF THE TcdA1 PORE COMPLEX EMBEDDED IN LIPID NANODISCS

In the following paragraph, we describe how we reconstituted the TcdA1 (TcA) component of the Tc toxin complex from *P. luminescens* into lipid nanodiscs and determined its structure using single-particle cryo-EM. Insecticidal Tc toxin complexes were first identified in *P. luminescens* (Bowen & Ensign, 1998; Bowen et al., 1998), but have later been found in other bacteria, including human pathogens. Tc toxin complexes are soluble virulence factors that perforate the host membrane similar to a syringe and translocate a toxic enzyme into the host cell. This damages and ultimately kills the host cell (Gatsogiannis et al., 2013; Lang et al., 2010). TcA (TcdA1 in *P. luminescens*), one of the three components of Tc complexes, forms a large pentameric structure with a molecular weight of 1.4 MDa. It is responsible for channel formation and the transfer of the biologically active enzyme into the host cell (Gatsogiannis et al., 2013; Meusch et al., 2014). Membrane insertion of TcA is triggered at low or high pH (Fig. 5A) (Gatsogiannis et al., 2013). Previously we solved the structure of TcdA1 from *P. luminescens* in the prepore state, i.e., before membrane penetration, by X-ray crystallography and cryo-EM (Gatsogiannis et al., 2013; Meusch et al., 2014). To obtain the structure of TcdA1 in the pore state, we shifted the pH level and simultaneously reconstituted the complex into liposomes. Single-particle cryo-EM analysis using a CMOS detector revealed the first structure of TcdA1 in a lipid bilayer (Fig. 5B) (Gatsogiannis et al., 2013). The resolution, however, of the resulting 3-D reconstruction was limited to 20 Å. This was probably due to the relatively thick ice layer resulting from the large diameter of the proteoliposomes, the strong signal of the membrane bilayer, and image drift.

In a later study (Meusch et al., 2014), we induced TcA pore formation in solution and stabilized the protein by detergent (0.05% Tween-20). Subsequently, we determined the structure of the complex at 9 Å by single-particle cryo-EM. However, already at the stage of 2-D classification, we noticed that the transmembrane domain appeared blurry, indicating that it was not sufficiently stabilized by the detergent (Fig. 5C). Consequently, the transmembrane domain was not resolved in the resulting 3-D volume (Fig. 5G).

To finally reveal the structure of the transmembrane region, we reconstituted the toxin complex into nanodiscs. Besides ensuring a native-like lipid environment, we anticipated that we could obtain more stable and

homogeneous TcA pore complexes suitable for high-resolution cryo-EM. According to our low-resolution studies of the TcA pore and the crystal structure of the prepore state, the outer diameter of the transmembrane domain measures ~40 Å. Therefore, we chose a small MSP construct, namely, MSP1D1, that forms nanodiscs with a diameter of 95–100 Å (Denisov et al., 2004). To test the suitability of POPC lipids for TcA insertion, we first reconstituted the protein in POPC liposomes and analyzed the reconstitution efficiency by negative stain EM.

In contrast to a typical detergent-solubilized membrane protein, the TcA pore conformation must be induced by shifting the pH before the protein can be reconstituted into nanodiscs. Therefore, we coupled the reconstitution process directly with a shift to a high pH. Based on the available low-resolution structure, we estimated the TcA pore membrane section to be 1300 $Å^2$, and as a starting point we used 110 lipids per nanodisc for the reconstitution. We also mixed protein, MSP, and lipids at various molar ratios and monitored the reconstitution success by SEC and negative stain EM. The best result was achieved with a large excess of empty nanodiscs (1 TcdA1: 4 nanodiscs), as described below. A detailed description of the reconstitution protocol follows:

- The POPC lipids were prepared as described for RyR1.
- TcdA1 from *P. luminescens* was cloned, overexpressed, and purified as described previously (Gatsogiannis et al., 2016). The final purification step was performed on a Superose 6 10/300 GL column (GE Healthcare Life Sciences) in a buffer containing 50 m*M* Tris–HCl, pH 8.0, 100 m*M* NaCl, and 0.05% Tween-20.
- POPC was solubilized at a concentration of 1 mg/mL in 10 m*M* MOPS, pH 7.4, 150 m*M* NaCl, and 10% CHAPS in order to use in nanodisc reconstitution.
- MSP1D1 was purchased from Cube Biotech (Germany) and solubilized in 20 m*M* Tris–HCl, pH 8, 250 m*M* NaCl, and 1% sodium cholate.
- MSP1D1 and POPC were incubated for 30 min in buffer containing 20 m*M* Tris–HCl, pH 8, 250 m*M* NaCl, and 1% (w/v) sodium cholate at 4°C.
- Reconstitution was performed by mixing TcdA1, MSP1D1, and POPC in a molar ratio of 1:8:440 in 20 m*M* Tris–HCl, pH 8, 250 m*M* NaCl, and 1% sodium cholate. After incubation for 1 h, the sample was dialyzed against buffer at pH 11 without detergents (20 m*M* CAPS, pH 11, and 250 m*M* NaCl) overnight at 4°C to induce the pH-dependent conformational change of TcdA1 and reconstitution into nanodiscs. We also

tried to remove the detergent by Bio-Beads instead of dialysis, but this resulted in a loss of a large amount of protein.
- The quality of the reconstituted TcdA1 protein in nanodiscs was checked by negative stain EM. Before the sample was used for cryo-EM, the TcdA1–nanodiscs were further purified by SEC using a Superose 6 column in 20 m*M* CAPS, pH 11, 250 m*M* NaCl.

A negative stain EM analysis directly after reconstitution revealed that one to three TcdA1 molecules were embedded in the same nanodisc. A large fraction of particles showed two TcdA1 proteins embedded from opposite sides. To isolate the population of nanodiscs harboring only a single TcdA1 molecule, we performed an additional purification step by SEC. This step also removed the excess of empty nanodiscs. We screened fractions of the elution peak by negative stain EM and used the best one for single-particle cryo-EM (Fig. 5F). Before vitrification, we added 0.01% fOM (Anatrace) to the buffer to obtain a homogeneous thickness of the amorphous ice. Subsequently, 4 μL of the sample (0.04 mg/mL) was applied to freshly glow-discharged carbon grids (C-flat, 2/1, Protochips), covered with a thin film of continuous carbon and vitrified after double-side blotting at 90% humidity by plunging into liquid ethane using a Cp3 (Cryoplunge3, Gatan).

We collected 1,957 movies with a Falcon II detector on a Cs-corrected Titan Krios (FEI) and manually selected ~30,000 TcdA1–nanodisc particles (for more details, see Gatsogiannis et al., 2016). The 2-D class averages showed the typical mushroom-shaped TcdA1 pores and a density corresponding to the nanodisc. The transmembrane channel surrounded by the nanodisc was clearly resolved and in an obvious open conformation (Fig. 5D). In contrast to detergent the native-like environment of the nanodisc induced the opening of the pore and stabilized the transmembrane channel in its open conformation. Moreover, the 2-D class averages showed a high level of structural detail, indicating that the nanodiscs did not negatively influence the image alignment.

We finally solved the 3-D structure of the TcdA1 pore at an average resolution of 3.5 Å (Fig. 5G) (Gatsogiannis et al., 2016). However, in contrast to other membrane proteins (Bai et al., 2015; Gao et al., 2016), the transmembrane domain was less resolved than the other domains. In an attempt to improve the resolution in the transmembrane region, we reselected the particles with the box center shifted to the center of the nanodisc and reextracted the particles in smaller boxes. Then we performed focused 2-D and 3-D classifications and subsequently a local refinement. The resolution of the transmembrane helices could not be improved, but

the analysis revealed that TcdA1 was positioned at different locations inside the nanodiscs. This indicates that the relatively large diameter of the nanodisc allows the protein to freely move inside the boundaries of the MSP (Fig. 5H). To find out why the resolution of the transmembrane helices was limited, we calculated MD simulations of this region in a model membrane. The simulations indicated that the transmembrane domain of the TcdA1 channel is very flexible and partially loses its fivefold symmetry. Thus, the lower local resolution in this area most likely does not stem from the "positional freedom" of this domain within the nanodisc, but is a result of an intrinsic flexibility of the domain. In addition, the MD simulations as well as the cryo-EM density indicated that, at the rim of the channel, lipids reach into the space between protomers, possibly stabilizing the open state. This could also explain the stabilizing effect of the nanodisc on the TcdA1 pore and their superiority over detergents for studying the pore conformation of Tc toxins (Fig. 5G).

5. CONCLUSIONS AND PERSPECTIVES

In this chapter, we have described advantages and practical methods for using lipid nanodiscs in structural studies of membrane proteins. While ensuring a native or a nearly native environment in which membrane proteins are fully functional, nanodiscs provide other possible advantages. Adding a molecular weight of more than 100 kDa, reconstitution into nanodiscs results in an increase of the overall size of the particle. This may be of particular advantage to single-particle cryo-EM of smaller membrane proteins, making it easier to image, select, and process them. However, the additional mass of the nanodisc will only be advantageous if their dimensional heterogeneity does not interfere with particle alignment. Unfortunately, nanodisc heterogeneity cannot be completely prevented at the moment especially if the nanodisc is chosen large enough to avoid unwanted interactions with the MSP. Therefore, it is challenging to study membrane proteins that have very small extramembrane domains. New image-processing algorithms and an improved nanodisc preparation will be needed to overcome this hurdle. In addition, increasing the contrast by taking images with a Volta phase plate could be beneficial. It will be interesting to explore the size limits of reconstituted proteins for high-resolution cryo-EM in the future.

The exposure of membrane proteins to detergents is reduced to a minimum when nanodiscs are used (Civjan et al., 2003; Duan et al., 2004; Marty

et al., 2013; Roy et al., 2015; Shirzad-Wasei et al., 2015). This is especially beneficial for the structural analysis of highly unstable membrane proteins or multisubunit membrane protein complexes that interact weakly or only transiently. The interaction of several membrane proteins reconstituted in the same nanodisc presents an exciting opportunity for structural studies (Boldog et al., 2006). Such a system would closely mimic a real biological membrane environment with 2-D protein diffusion under crowded conditions and would be ideal to study at high-resolution processes, such as signal transduction, involving formation of transient complexes.

It remains to be seen how well other lipid-containing bilayer mimetics, in particular those based on SMA instead of MSP and liposomes, are suited for high-resolution single-particle cryo-EM. If both of these alternatives work, they would beautifully complement the MSP-based nanodisc system and together equip structural biologists with powerful tools for studying membrane proteins in a near to native environment.

ACKNOWLEDGMENTS

This work was funded by Vlaams Instituut voor Biotechnologie (to R.E.), Humboldt Foundation (to R.E.), Fonds voor Wetenschappelijk Onderzoek Vlaanderen (grant number G.0266.15N to R.E.), Max Planck Society (to S.R.), and the European Council under the European Union's Seventh Framework Programme (FP7/2007–2013) (grant no. 615984 to S.R.).

REFERENCES

Allegretti, M., Klusch, N., Mills, D. J., Vonck, J., Kühlbrandt, W., & Davies, K. M. (2015). Horizontal membrane-intrinsic α-helices in the stator *a*-subunit of an F-type ATP synthase. *Nature*, *521*, 237–240. http://dx.doi.org/10.1038/nature14185.

Bai, X.-C., Yan, Z., Wu, J., Li, Z., & Yan, N. (2016). The central domain of RyR1 is the transducer for long-range allosteric gating of channel opening. *Cell Research*, *26*, 995–1006. http://dx.doi.org/10.1038/cr.2016.89.

Bai, X.-C., Yan, C., Yang, G., Lu, P., Ma, D., Sun, L., et al. (2015). An atomic structure of human γ-secretase. *Nature*, *525*, 212–217. http://dx.doi.org/10.1038/nature14892.

Bao, H., Dalal, K., Wang, V., Rouiller, I., & Duong, F. (2013). The maltose ABC transporter: Action of membrane lipids on the transporter stability, coupling and ATPase activity. *Biochimica Et Biophysica Acta (BBA)-Biomembranes*, *1828*, 1723–1730. http://dx.doi.org/10.1016/j.bbamem.2013.03.024.

Bao, H., & Duong, F. (2014). Nucleotide-free MalK drives the transition of the maltose transporter to the inward-facing conformation. *Journal of Biological Chemistry*, *289*, 9844–9851. http://dx.doi.org/10.1074/jbc.M113.545525.

Bayburt, T. H., Grinkova, Y. V., & Sligar, S. G. (2006). Assembly of single bacteriorhodopsin trimers in bilayer nanodiscs. *Archives of Biochemistry and Biophysics*, *450*, 215–222. http://dx.doi.org/10.1016/j.abb.2006.03.013.

Bayburt, T. H., & Sligar, S. G. (2003). Self-assembly of single integral membrane proteins into soluble nanoscale phospholipid bilayers. *Protein Science*, *12*, 2476–2481. http://dx.doi.org/10.1110/ps.03267503.

Boldog, T., Boldog, T., Grimme, S., Grimme, S., Li, M., Li, M., et al. (2006). Nanodiscs separate chemoreceptor oligomeric states and reveal their signaling properties. *Proceedings of the National Academy of Sciences of the United States of America*, *103*, 11509–11514. http://dx.doi.org/10.1073/pnas.0604988103.

Bowen, D. J., & Ensign, J. C. (1998). Purification and characterization of a high-molecular-weight insecticidal protein complex produced by the entomopathogenic bacterium *Photorhabdus luminescens*. *Applied and Environmental Microbiology*, *64*, 3029–3035.

Bowen, D., Rocheleau, T. A., Blackburn, M., Andreev, O., Golubeva, E., Bhartia, R., et al. (1998). Insecticidal toxins from the bacterium *Photorhabdus luminescens*. *Science*, *280*, 2129–2132.

Breyton, C., Chabaud, E., Chaudier, Y., Pucci, B., & Popot, J.-L. (2004). Hemifluorinated surfactants: A non-dissociating environment for handling membrane proteins in aqueous solutions? *FEBS Letters*, *564*, 312–318. http://dx.doi.org/10.1016/S0014-5793(04)00227-3.

Brilot, A. F., Chen, J. Z., Cheng, A., Pan, J., Harrison, S. C., Potter, C. S., et al. (2012). Beam-induced motion of vitrified specimen on holey carbon film. *Journal of Structural Biology*, *177*, 630–637. http://dx.doi.org/10.1016/j.jsb.2012.02.003.

Civjan, N. R., Bayburt, T. H., Schuler, M. A., & Sligar, S. G. (2003). Direct solubilization of heterologously expressed membrane proteins by incorporation into nanoscale lipid bilayers. *BioTechniques*, *35*, 556–563.

Crichton, P. G., Crichton, P. G., Harding, M., Harding, M., Ruprecht, J. J., Ruprecht, J. J., et al. (2013). Lipid, detergent, and Coomassie blue G-250 affect the migration of small membrane proteins in blue native gels: Mitochondrial carriers migrate as monomers not dimers. *The Journal of Biological Chemistry*, *288*, 22163–22173. http://dx.doi.org/10.1074/jbc.M113.484329.

Cross, T. A., Murray, D. T., & Watts, A. (2013). Helical membrane protein conformations and their environment. *European Biophysics Journal*, *42*, 731–755. http://dx.doi.org/10.1007/s00249-013-0925-x.

Das, A., & Sligar, S. G. (2009). Modulation of the cytochrome P450 reductase redox potential by the phospholipid bilayer. *Biochemistry*, *48*, 12104–12112. http://dx.doi.org/10.1021/bi9011435.

Deisenhofer, J., Epp, O., Miki, K., Huber, R., & Michel, H. (1985). Structure of the protein subunits in the photosynthetic reaction centre of *Rhodopseudomonas viridis* at 3Å resolution. *Nature*, *318*, 618–624.

Denisov, I. G., Grinkova, Y. V., Lazarides, A. A., & Sligar, S. G. (2004). Directed self-assembly of monodisperse phospholipid bilayer nanodiscs with controlled size. *Journal of the American Chemical Society*, *126*, 3477–3487. http://dx.doi.org/10.1021/ja0393574.

Denisov, I. G., McLean, M. A., Shaw, A. W., Grinkova, Y. V., & Sligar, S. G. (2005). Thermotropic phase transition in soluble nanoscale lipid bilayers. *The Journal of Physical Chemistry. B*, *109*, 15580–15588. http://dx.doi.org/10.1021/jp051385g.

Dörr, J. M., Koorengevel, M. C., Schäfer, M., Prokofyev, A. V., Scheidelaar, S., van der Cruijsen, E. A. W., et al. (2014). Detergent-free isolation, characterization, and functional reconstitution of a tetrameric K^+ channel: The power of native nanodiscs. *Proceedings of the National Academy of Sciences of the United States of America*, *111*, 18607–18612. http://dx.doi.org/10.1073/pnas.1416205112.

Dörr, J. M., Scheidelaar, S., Koorengevel, M. C., Dominguez, J. J., Schäfer, M., van Walree, C. A., et al. (2016). The styrene-maleic acid copolymer: A versatile tool in membrane research. *European Biophysics Journal*, *45*, 3–21. http://dx.doi.org/10.1007/s00249-015-1093-y.

Duan, H., Civjan, N. R., Sligar, S. G., & Schuler, M. A. (2004). Co-incorporation of heterologously expressed Arabidopsis cytochrome P450 and P450 reductase into soluble nanoscale lipid bilayers. *Archives of Biochemistry and Biophysics*, *424*, 141–153. http://dx.doi.org/10.1016/j.abb.2004.02.010.

Efremov, R. G., Leitner, A., Aebersold, R., & Raunser, S. (2015). Architecture and conformational switch mechanism of the ryanodine receptor. *Nature*, *517*, 39–43. http://dx.doi.org/10.1038/nature13916.

Eggensperger, S., Fisette, O., Parcej, D., et al. (2014). An annular lipid belt is essential for allosteric coupling and viral inhibition of the antigen translocation complex TAP (transporter associated with antigen processing). *The Journal of Biological Chemistry*, *289*, 33098–33108. http://dx.doi.org/10.1074/jbc.M114.592832.

Fiedorczuk, K., Letts, J. A., Degliesposti, G., Kaszuba, K., Skehel, M., & Sazanov, L. A. (2016). Atomic structure of the entire mammalian mitochondrial complex I. *Nature*, *538*, 406–410. http://dx.doi.org/10.1038/nature19794.

Frauenfeld, J., Gumbart, J., Sluis, E. O. V. D., Funes, S., Gartmann, M., Beatrix, B., et al. (2011). Cryo-EM structure of the ribosome-SecYE complex in the membrane environment. *Nature Structural & Molecular Biology*, *18*, 614–621. http://dx.doi.org/10.1038/nsmb.2026.

Frauenfeld, J., Löving, R., Armache, J.-P., Sonnen, A. F.-P., Guettou, F., Moberg, P., et al. (2016). A saposin-lipoprotein nanoparticle system for membrane proteins. *Nature Methods*, *13*, 345–351. http://dx.doi.org/10.1038/nmeth.3801.

Gao, Y., Cao, E., Julius, D., & Cheng, Y. (2016). TRPV1 structures in nanodiscs reveal mechanisms of ligand and lipid action. *Nature*, *534*, 347–351. http://dx.doi.org/10.1038/nature17964.

Gatsogiannis, C., Lang, A. E., Meusch, D., Pfaumann, V., Hofnagel, O., Benz, R., et al. (2013). A syringe-like injection mechanism in *Photorhabdus luminescens* toxins. *Nature*, *495*, 520–523. http://dx.doi.org/10.1038/nature11987.

Gatsogiannis, C., Merino, F., Prumbaum, D., Roderer, D., Leidreiter, F., Meusch, D., et al. (2016). Membrane insertion of a Tc toxin in near-atomic detail. *Nature Structural & Molecular Biology*, *23*, 884–890. http://dx.doi.org/10.1038/nsmb.3281.

Grinkova, Y. V., Denisov, I. G., & Sligar, S. G. (2010). Engineering extended membrane scaffold proteins for self-assembly of soluble nanoscale lipid bilayers. *Protein Engineering Design and Selection*, *23*, 843–848. http://dx.doi.org/10.1093/protein/gzq060.

Gupta, K., Donlan, J. A. C., Hopper, J. T. S., Uzdavinys, P., Landreh, M., Struwe, W. B., et al. (2017). The role of interfacial lipids in stabilizing membrane protein oligomers. *Nature*, *541*, 421–424. http://dx.doi.org/10.1038/nature20820.

Hagn, F., & Wagner, G. (2015). Structure refinement and membrane positioning of selectively labeled OmpX in phospholipid nanodiscs. *Journal of Biomolecular NMR*, *61*, 249–260. http://dx.doi.org/10.1007/s10858-014-9883-6.

Hawkes, M. J., Díaz-Muñoz, M., & Hamilton, S. L. (1989). A procedure for purification of the ryanodine receptor from skeletal muscle. *Membrane Biochemistry*, *8*, 133–145. http://eutils.ncbi.nlm.nih.gov/entrez/eutils/elink.fcgi?dbfrom=pubmed&id=2641949&retmode=ref&cmd=prlinks.

Hernández-Rocamora, V. M., García-Montañés, C., Rivas, G., & Llorca, O. (2012). Reconstitution of the *Escherichia coli* cell division ZipA–FtsZ complexes in nanodiscs as revealed by electron microscopy. *Journal of Structural Biology*, *180*, 531–538. http://dx.doi.org/10.1016/j.jsb.2012.08.013.

Hiller, S., & Wagner, G. (2009). The role of solution NMR in the structure determinations of VDAC-1 and other membrane proteins. *Current Opinion in Structural Biology*, *19*, 396–401. http://dx.doi.org/10.1016/j.sbi.2009.07.013.

Hohn, M., Tang, G., Goodyear, G., Baldwin, P. R., Huang, Z., Penczek, P. A., et al. (2007). SPARX, a new environment for cryo-EM image processing. *Journal of Structural Biology*, *157*, 47–55. http://dx.doi.org/10.1016/j.jsb.2006.07.003.

Ilgü, H., Jeckelmann, J.-M., Gachet, M. S., Boggavarapu, R., Ucurum, Z., Gertsch, J., et al. (2014). Variation of the detergent-binding capacity and phospholipid content of membrane proteins when purified in different detergents. *Biophysical Journal*, *106*, 1660–1670. http://dx.doi.org/10.1016/j.bpj.2014.02.024.

Johnson, P. J. M., Halpin, A., Morizumi, T., Brown, L. S., Prokhorenko, V. I., Ernst, O. P., et al. (2014). The photocycle and ultrafast vibrational dynamics of bacteriorhodopsin in lipid nanodiscs. *Physical Chemistry Chemical Physics*, *16*, 21310–21320. http://dx.doi.org/10.1039/c4cp01826e.

Justesen, B. H., Justesen, B. H., Hansen, R. W., Hansen, R. W., Martens, H. J., Martens, H. J., et al. (2013). Active plasma membrane P-type H^+-ATPase reconstituted into nanodiscs is a monomer. *The Journal of Biological Chemistry*, *288*, 26419–26429. http://dx.doi.org/10.1074/jbc.M112.446948.

Kawai, T., Caaveiro, J. M. M., Abe, R., Katagiri, T., & Tsumoto, K. (2011). Catalytic activity of MsbA reconstituted in nanodisc particles is modulated by remote interactions with the bilayer. *FEBS Letters*, *585*, 3533–3537. http://dx.doi.org/10.1016/j.febslet.2011.10.015.

Kim, J., Wu, S., Tomasiak, T. M., Mergel, C., Winter, M. B., Stiller, S. B., et al. (2015). Subnanometre-resolution electron cryomicroscopy structure of a heterodimeric ABC exporter. *Nature*, *517*, 396–400. http://dx.doi.org/10.1038/nature13872.

Kühlbrandt, W. (2014). The resolution revolution. *Science*, *343*, 1443–1444. http://dx.doi.org/10.1126/science.1251652.

Lam, E., & Packer, L. (1983). Nonionic detergent effects on spectroscopic characteristics and the photocycle of bacteriorhodopsin in purple membranes. *Archives of Biochemistry and Biophysics*, *221*, 557–564.

Lang, A. E., Schmidt, G., Schlosser, A., Hey, T. D., Larrinua, I. M., Sheets, J. J., et al. (2010). *Photorhabdus luminescens* toxins ADP-ribosylate actin and RhoA to force actin clustering. *Science*, *327*, 1139–1142. http://dx.doi.org/10.1126/science.1184557.

Lee, A. (2004). How lipids affect the activities of integral membrane proteins. *Biochimica Et Biophysica Acta (BBA)-Biomembranes*, *1666*, 62–87. http://dx.doi.org/10.1016/j.bbamem.2004.05.012.

Lee, T.-Y., Yeh, V., Chuang, J., Chung Chan, J. C., Chu, L.-K., & Yu, T.-Y. (2015). Tuning the photocycle kinetics of bacteriorhodopsin in lipid nanodiscs. *Biophysical Journal*, *109*, 1899–1906. http://dx.doi.org/10.1016/j.bpj.2015.09.012.

Leitz, A. J., Bayburt, T. H., Barnakov, A. N., Springer, B. A., & Sligar, S. G. (2006). Functional reconstitution of β_2-adrenergic receptors utilizing self-assembling nanodisc technology. *BioTechniques*, *40*, 601–612. http://dx.doi.org/10.2144/000112169.

Letts, J. A., Fiedorczuk, K., & Sazanov, L. A. (2016). The architecture of respiratory supercomplexes. *Nature*, *537*, 644–648. http://dx.doi.org/10.1038/nature19774.

Lévy, D., Rigaud, J. L., Lévy, D., Mosser, G., Lambert, O., Mosser, G., et al. (1999). Two-dimensional crystallization on lipid layer: A successful approach for membrane proteins. *Journal of Structural Biology*, *127*, 44–52. http://dx.doi.org/10.1006/jsbi.1999.4155.

Li, X., Mooney, P., Zheng, S., Booth, C. R., Braunfeld, M. B., Gubbens, S., et al. (2013). Electron counting and beam-induced motion correction enable near-atomic-resolution single-particle cryo-EM. *Nature Methods*, *10*, 584–590. http://dx.doi.org/10.1038/nmeth.2472.

Liao, M., Cao, E., Julius, D., & Cheng, Y. (2013). Structure of the TRPV1 ion channel determined by electron cryo-microscopy. *Nature*, *504*, 107–112. http://dx.doi.org/10.1038/nature12822.

Marty, M. T., Wilcox, K. C., Klein, W. L., & Sligar, S. G. (2013). Nanodisc-solubilized membrane protein library reflects the membrane proteome. *Analytical and Bioanalytical Chemistry*, *405*, 4009–4016. http://dx.doi.org/10.1007/s00216-013-6790-8.

Matthies, D., Dalmas, O., Borgnia, M. J., Dominik, P. K., Merk, A., Rao, P., et al. (2016). Cryo-EM structures of the magnesium channel CorA reveal symmetry break upon gating. *Cell*, *164*, 747–756. http://dx.doi.org/10.1016/j.cell.2015.12.055.

McMullan, G., Faruqi, A. R., Clare, D., & Henderson, R. (2014). Comparison of optimal performance at 300 keV of three direct electron detectors for use in low dose electron microscopy. *Ultramicroscopy*, *147*, 156–163. http://dx.doi.org/10.1016/j.ultramic.2014.08.002.

Meusch, D., Gatsogiannis, C., Efremov, R. G., Lang, A. E., Hofnagel, O., Vetter, I. R., et al. (2014). Mechanism of Tc toxin action revealed in molecular detail. *Nature*, *508*, 61–65. http://dx.doi.org/10.1038/nature13015.

Mi, L.-Z., Grey, M. J., Nishida, N., Walz, T., Lu, C., & Springer, T. A. (2008). Functional and structural stability of the epidermal growth factor receptor in detergent micelles and phospholipid nanodiscs. *Biochemistry*, *47*, 10314–10323. http://dx.doi.org/10.1021/bi801006s.

Nagle, J. F., & Tristram-Nagle, S. (2000). Structure of lipid bilayers. *Biochimica et Biophysica Acta*, *1469*, 159–195. http://eutils.ncbi.nlm.nih.gov/entrez/eutils/elink.fcgi?dbfrom=pubmed&id=11063882&retmode=ref&cmd=prlinks.

Nasr, M. L., Baptista, D., Strauss, M., Sun, Z.-Y. J., Grigoriu, S., Huser, S., et al. (2017). Covalently circularized nanodiscs for studying membrane proteins and viral entry. *Nature Methods*, *14*, 49–52. http://dx.doi.org/10.1038/nmeth.4079.

Nasr, M. L., & Singh, S. K. (2014). Radioligand binding to nanodisc-reconstituted membrane transporters assessed by the scintillation proximity assay. *Biochemistry*, *53*, 4–6. http://dx.doi.org/10.1021/bi401412e.

Orlando, B. J., McDougle, D. R., Lucido, M. J., Eng, E. T., Graham, L. A., Schneider, C., et al. (2014). Cyclooxygenase-2 catalysis and inhibition in lipid bilayer nanodiscs. *Archives of Biochemistry and Biophysics*, *546*, 33–40. http://dx.doi.org/10.1016/j.abb.2014.01.026.

Overington, J. P., Al-Lazikani, B., & Hopkins, A. L. (2006). How many drug targets are there? *Nature Reviews. Drug Discovery*, *5*, 993–996. http://dx.doi.org/10.1038/nrd2199.

Phillips, R., Ursell, T., Wiggins, P., & Sens, P. (2009). Emerging roles for lipids in shaping membrane-protein function. *Nature*, *459*, 379–385. http://dx.doi.org/10.1038/nature08147.

Popot, J.-L., Althoff, T., Bagnard, D., Banères, J.-L., Bazzacco, P., Billon-Denis, E., et al. (2011). Amphipols from A to Z. *Annual Review of Biophysics*, *40*, 379–408. http://dx.doi.org/10.1146/annurev-biophys-042910-155219.

Raunser, S., & Walz, T. (2009). Electron crystallography as a technique to study the structure on membrane proteins in a lipidic environment. *Annual Review of Biophysics*, *38*, 89–105. http://dx.doi.org/10.1146/annurev.biophys.050708.133649.

Ritchie, T. K., Grinkova, Y. V., Bayburt, T. H., Denisov, I. G., Zolnerciks, J. K., Atkins, W. M., et al. (2009). Chapter 11—Reconstitution of membrane proteins in phospholipid bilayer nanodiscs. *Methods in Enzymology*, *464*, 211–231. http://dx.doi.org/10.1016/S0076-6879(09)64011-8.

Roy, J., Pondenis, H., Fan, T. M., & Das, A. (2015). Direct capture of functional proteins from mammalian plasma membranes into nanodiscs. *Biochemistry*, *54*, 6299–6302. http://dx.doi.org/10.1021/acs.biochem.5b00954.

Samsó, M., Feng, W., Pessah, I. N., & Allen, P. D. (2009). Coordinated movement of cytoplasmic and transmembrane domains of RyR1 upon gating. *PLoS Biology, 7*, e85. http://dx.doi.org/10.1371/journal.pbio.1000085.sv002.

Samsó, M., Wagenknecht, T., & Allen, P. D. (2005). Internal structure and visualization of transmembrane domains of the RyR1 calcium release channel by cryo-EM. *Nature Structural & Molecular Biology*, *12*, 539–544. http://dx.doi.org/10.1038/nsmb938.

Scheidelaar, S., Koorengevel, M. C., Pardo, J. D., Meeldijk, J. D., Breukink, E., & Killian, J. A. (2015). Molecular model for the solubilization of membranes into nanodisks by styrene maleic acid copolymers. *Biophysical Journal*, *108*, 279–290. http://dx.doi.org/10.1016/j.bpj.2014.11.3464.

Schmidt-Krey, I., & Rubinstein, J. L. (2011). Electron cryomicroscopy of membrane proteins: Specimen preparation for two-dimensional crystals and single particles. *Micron*, *42*, 107–116. http://dx.doi.org/10.1016/j.micron.2010.07.004.

Schuler, M. A., Denisov, I. G., & Sligar, S. G. (2013). Nanodiscs as a new tool to examine lipid-protein interactions. *Methods in Molecular Biology*, *974*, 415–433. http://dx.doi.org/10.1007/978-1-62703-275-9_18.

Shen, P. S., Yang, X., DeCaen, P. G., Liu, X., Bulkley, D., Clapham, D. E., et al. (2016). The structure of the polycystic kidney disease channel PKD2 in lipid nanodiscs. *Cell*, *167*. 763–773.e11. http://dx.doi.org/10.1016/j.cell.2016.09.048.

Shih, A. Y., Denisov, I. G., Phillips, J. C., Sligar, S. G., & Schulten, K. (2005). Molecular dynamics simulations of discoidal bilayers assembled from truncated human lipoproteins. *Biophysical Journal*, *88*, 548–556. http://dx.doi.org/10.1529/biophysj.104.046896.

Shirzad-Wasei, N., van Oostrum, J., Bovee-Geurts, P. H. M., Kusters, L. J. A., Bosman, G. J. C. G. M., & DeGrip, W. J. (2015). Rapid transfer of overexpressed integral membrane protein from the host membrane into soluble lipid nanodiscs without previous purification. *Biological Chemistry*, *396*, 1–13. http://dx.doi.org/10.1515/hsz-2015-0100.

Stepien, P., Polit, A., & Wisniewska-Becker, A. (2015). Comparative EPR studies on lipid bilayer properties in nanodiscs and liposomes. *Biochimica et Biophysica Acta*, *1848*, 60–66. http://dx.doi.org/10.1016/j.bbamem.2014.10.004.

Uhlén, M., Fagerberg, L., Hallström, B. M., Lindskog, C., Oksvold, P., Mardinoglu, A., et al. (2015). Tissue-based map of the human proteome. *Science*, *347*, 1260419. http://dx.doi.org/10.1126/science.1260419.

Urbani, A., & Warne, T. (2005). A colorimetric determination for glycosidic and bile salt-based detergents: Applications in membrane protein research. *Analytical Biochemistry*, *336*, 117–124. http://dx.doi.org/10.1016/j.ab.2004.09.040.

Van Petegem, F. (2014). Ryanodine receptors: Allosteric ion channel giants. *Journal of Molecular Biology*, 1–23. http://dx.doi.org/10.1016/j.jmb.2014.08.004.

Vinothkumar, K. R., & Henderson, R. (2010). Structures of membrane proteins. *Quarterly Reviews of Biophysics*, *43*, 65–158. http://dx.doi.org/10.1017/S0033583510000041.

Wadsäter, M., Maric, S., Simonsen, J. B., Mortensen, K., Bendall, D. S., & Cárdenas, M. (2013). The effect of using binary mixtures of zwitterionic and charged lipids on nanodisc formation and stability. *Soft Matter*, *9*, 2329. http://dx.doi.org/10.1039/c2sm27000e.

Wang, L., & Sigworth, F. J. (2010). Liposomes on a streptavidin crystal: A system to study membrane proteins by cryo-EM. *Methods in Enzymology*, *481*, 147–164. http://dx.doi.org/10.1016/S0076-6879(10)81007-9.

Wu, M., Gu, J., Guo, R., Huang, Y., & Yang, M. (2016). Structure of mammalian respiratory supercomplex I1III2IV1. *Cell*, *167*. 1598–1609.e10. http://dx.doi.org/10.1016/j.cell.2016.11.012.

Wu, J., Yan, Z., Li, Z., Qian, X., Lu, S., Dong, M., et al. (2016). Structure of the voltage-gated calcium channel Cav1.1 at 3.6 Å resolution. *Nature*, *537*, 191–196. http://dx.doi.org/10.1038/nature19321.

Yan, Z., Bai, X.-C., Yan, C., Wu, J., Li, Z., Xie, T., et al. (2015). Structure of the rabbit ryanodine receptor RyR1 at near-atomic resolution. *Nature*, *517*, 50–55. http://dx.doi.org/10.1038/nature14063.

Yeagle, P. L. (2014). Non-covalent binding of membrane lipids to membrane proteins. *Biochimica et Biophysica Acta*, *1838*, 1548–1559. http://dx.doi.org/10.1016/j.bbamem.2013.11.009.

Yuchi, Z., & Van Petegem, F. (2016). Ryanodine receptors under the magnifying lens: Insights and limitations of cryo-electron microscopy and X-ray crystallography studies. *Cell Calcium*, *59*, 209–227. http://dx.doi.org/10.1016/j.ceca.2016.04.003.

Zalk, R., Clarke, O. B., Georges, A. d., Grassucci, R. A., Reiken, S., Mancia, F., et al. (2015). Structure of a mammalian ryanodine receptor. *Nature*, *517*, 44–49. http://dx.doi.org/10.1038/nature13950.

Zhou, H.-X., & Cross, T. A. (2013). Influences of membrane mimetic environments on membrane protein structures. *Annual Review of Biophysics*, *42*, 361–392. http://dx.doi.org/10.1146/annurev-biophys-083012-130326.

Zhu, J., Vinothkumar, K. R., & Hirst, J. (2016). Structure of mammalian respiratory complex I. *Nature*, *536*, 354–358. http://dx.doi.org/10.1038/nature19095.